Chapter 3
Design of FOPID controller using Nelder-Mead algorithm

3.1 Introduction

Nowadays, numerous optimization techniques are available for nonlinear functions that can't be solved analytically. These techniques are essentially iterative in nature and the user have to guess some initial or starting positions of the desired parameters. Most of these techniques engage first order or second order derivatives to decide the searching route to enhance the value of fitness function. Most of the techniques for nonlinear function are referred in books by Fletcher, Gill, Murray, and Wright and Luenberger [52]. These existing techniques "are totally deterministic in nature when applied to problems affected by 'noise', but the error occurs in measurement or ambiguity in prediction and hence they are either unable to attain an optimum solution or in worst case they may achieve a false solution" [52].

There are other techniques that are specially designed to converge globally to a local optimizer in presence of some noise under certain conditions. These techniques are known as stochastic approximation methods, pioneered by Robbins and Monro.

Different from the derivative-based and stochastic approximation methods, there exists a class of techniques known as direct-search methods. In contrast to other optimization techniques, direct-search algorithms depend wholly on the value of the fitness function on a set of points. The advantages of direct-search methods over derivative-based methods include:

- Requirement of simple calculations.
- Demand of relatively low storage.

- Need less adjustable parameters.
- The algorithms are effective when evaluation errors are significant because they operate on the worst rather than the best point.

In this chapter a renowned heuristic direct-search techniques known as Nelder-Mead algorithm or simplex search algorithm is elaborated for optimization of FOPID controller parameters for different systems.

3.2 Nelder-Mead Algorithm

The Nelder-Mead algorithm or simplex search algorithm is designed from geometric intuition and comes under heuristic direct-search techniques. The algorithm was presented in 1965 by Nelder and Mead. The basic concept of the algorithm is relatively simple to understand and to implement. Easiness of implementation and low storage constraints, help the algorithm gain reputation very quickly. This resulted its acceptance in various fields of science and technology, and particularly in chemistry and medicine. Despite of its age and recently developed advanced algorithms in direct search methods domain, the Nelder-Mead optimization is still one of the most popular algorithm in practice. Apart from minor computational steps in the basic algorithm, the major variation between various realizations is in the construction of the initial simplex, and selection of convergence or execution tests performed at the end of the iteration routine.

Nelder and Mead's algorithm starts with the function's values on a set of $(n + 1)$ points in the search space, where n represents the number of variables in function to be optimized. These points in the search space define a polytope in $\Re^n$ which has $(n + 1)$ vertices known as simplex. The algorithm then passes through a sequence of operations on the simplex to push it probably toward a local optimum. If the optimum is minimum then the algorithm replaces the worst vertex of the simplex with a new vertex that has a lesser function value by using anyone of the operations namely: reflection, expansion or

contraction. If none of these operations is able to locate a new vertex to substitute the worst vertex in the search space, then the whole simplex diminish towards the vertex with the smallest function value. A standard form of the rules for function minimization is given as:

(i) Initialization of simplex:

Initial simplex is formed by choosing $(n + 1)$ points for a function having n parameters in the search space. Normally the initial simplex is a regular polytope consisting of $(n + 1)$ sides (e.g. an equilateral triangle in case of 2 parameters, a regular tetrahedron in case of 3 parameters, etc.). Further, function value at each vertices of the simplex is calculated and ranked according to ascending order of their function values. That is, if v_1 is the vertex having lowest function value, v_2 is the vertex having second lowest function value and so on, then the order will be like $(v_1, v_2, v_3, \ldots\ldots, v_n, v_{n+1})$. Let this set is denoted by the order set S_0.

(ii) Simplex upgrade:

Let k is the iteration number of the particular step which is started by eliminating the vertex having highest function value v^{n+1} from the present simplex S^{k-1}. Then locate the centroid of the existing n set points of S^{k-1}, which will be denoted by $v_{centroid}$. The centroid of n points is calculated as:

$$v_{centroid} = \frac{1}{n}\sum_{i=1}^{n} v_i \tag{3.1}$$

Thereafter, a new point is generated by reflecting v_{n+1} through $v_{centroid}$ by using the relation given below:

$$v_{reflect} = (1+\ell)v_{centroid} - \ell v_{n+1} \tag{3.2}$$

where ℓ is the reflection coefficient typically considered to be 1. Then depending upon the rank of $v_{centroid}$, among the other vertices the Expansion, Reflection, or Contraction

will be performed on the current simplex S^{k-1} which is discussed below. Figure 3.1 illustrates these operations.

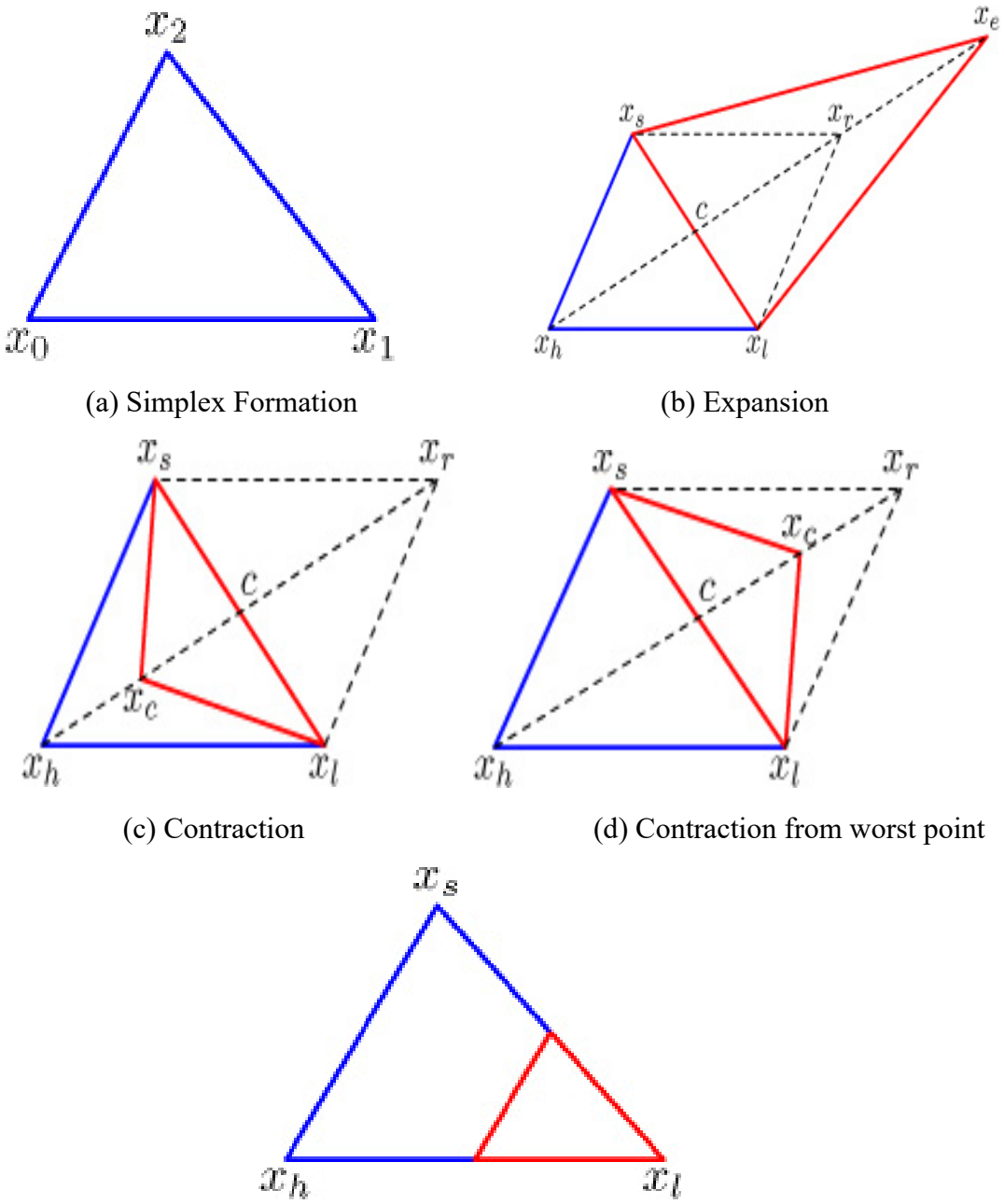

(a) Simplex Formation (b) Expansion

(c) Contraction (d) Contraction from worst point

(e) Shrinking using worst point

Fig. 3.1. Different steps of simplex upgradation

a) Expansion

If $v_{reflect} < v_1$ then the reflection is extended in the identical direction using the Equation 3.3:

. $$v_{\exp and} = \rho v_{reflect} + (1-\rho)v_{centroid} \quad (3.3)$$

where ρ is the expansion coefficient and normally assumed to be 2.

i. Accept: If $v_{\exp and} < v_1$, then $v_{\exp and}$ substitutes v_{n+1} in the simplex.

ii. Reject: else $v_{reflect}$ substitutes v_{n+1} in the simplex.

b) Reflection:

If $v_1 \le v_{reflect} \le v_n$, then $v_{reflect}$ is kept in place of v_{n+1} in the simplex.

c) Contraction:

In other case when $v_{reflect} > v_n$, then a contraction take place. In this process if $v_{reflect} \le v_{n+1}$, then $v_{reflect}$ is replaced by v_{n+1} before a shrinkage is performed. The contraction vertex can be measured by using Equation 3.4.

$$v_{contract} = \partial v_{n+1} + (1-\partial)\, v_{\text{centroid}} \quad (3.4)$$

where ∂ is the coefficient of contraction and generally considered to be $\frac{1}{2}$.

i. Accept: If $v_{contract} \le v_{n+1}$, then v_{n+1} will be replaced by $v_{contract}$ in the simplex.

ii. Reject: otherwise, shrink the whole simplex towards v_1 by replacing each vertices v_i for $i = 2,3.....,(n+1)$, by using Equation 3.5 below.

$$v_i = \eta v_i + (1-\eta)v_1 \quad (3.5)$$

where η is the coefficient of shrinking and generally assumed to be $\frac{1}{2}$.

(iii)Termination or return to stage upgrade:

At this stage either a fresh vertex replaces the vertex v_{n+1} followed by a reflection, an expansion, or a contraction or n new vertices have replaced all the vertices v_i for $i = 2,3.....,(n+1)$ by a shrinking process. Now, new set of vertices are reordered in ascending order of their function values and this fresh set is denoted as S^k. So the simplex is at the closing stage of the k^{th} iteration.

Hence, if the ending criterion is satisfied, the program will be terminated; else, another iteration of the upgrade stage will be executed.

The generalized formulation of NM-algorithms is illustrated here. It's enhanced version towards FOPID (which is having five variable to optimize simultaneously) is implemented in this work by optimizing the FOPID controller parameters designed for various systems. In the proposed algorithm ISE is used as the fitness function and best result is considered after 100 iterations in every case of optimization. Optimizing FOPID controller parameters using NM-algorithm for various systems is elaborated ahead in this chapter accordingly.

3.3 Illustrative Examples

3.3.1 Design of an FOPID controller for a third order linear plant

Consider the third order plant given by continuous time open loop transfer function [59].

$$G(s) = \frac{0.6s^2 + 3s + 3.75}{0.4s^3 + 1.6s^2 + 3s + 3.75} \tag{3.6}$$

The system has its predefined requirements for the proposed controller which are given as:

- $Gain\ margin\ > 6\ dB$
- $Phase\ margin = [60^{\circ} - 90^{\circ}]$
- $Settling\ time\ < 1sec.$
- $Peak\ overshoot\ < 10\%$

The step-response of the unity feedback closed-loop system without controller is shown in Figure 3.2. It is observed that the closed-loop response depicts a large steady state error and settling time of more than 2 seconds. Thus, to fulfill the design requirements an efficient controller is desired. In this concern, primarily an integer order PID controller is designed using ZN-method to extract an appropriate search space for the proposed algorithm to design the FOPID controller for the considered plant.

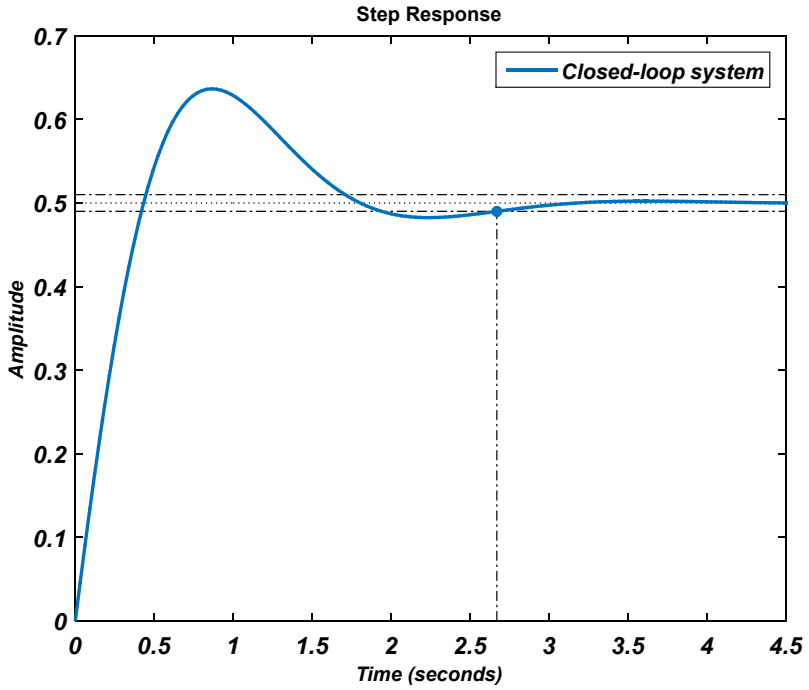

Fig. 3.2. Step response of the closed-loop system without controller.

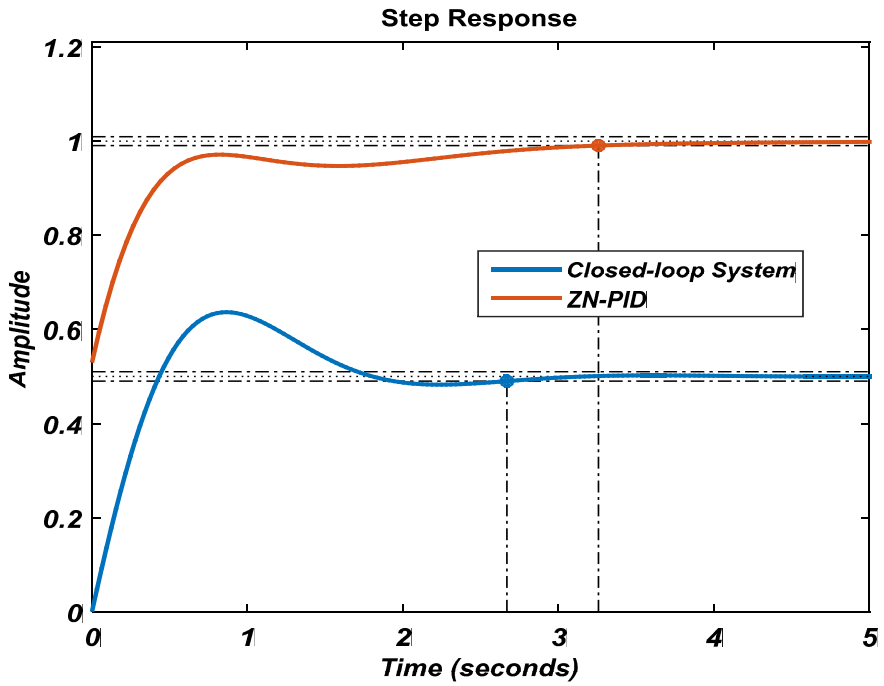

Fig. 3.3. Step response of the closed-loop system with ZN-PID

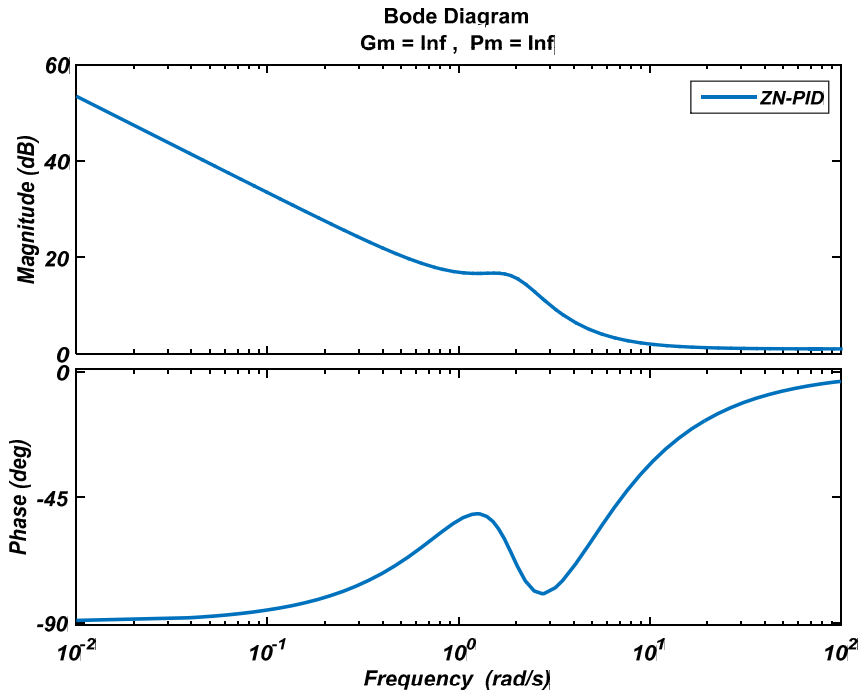

Fig. 3.4. Frequency response of the system with ZN-PID

Figure 3.3 presents the classical PID controller designed using ZN-method (i.e. ZN-PID). It showcase the reduction in steady state error of the system but increases the settling time of the system to the higher value. Simultaneously, the frequency response of the system shown in Figure 3.4 show an infinite gain and phase margin which is not required.

Here, an FOPID controller is designed by taking the starting value of different gain constants ($i.e.\ K_P, K_I,$ and K_D) from ZN-method and the fractional power terms ($i.e.\ \lambda$ and μ) are chosen randomly. After optimization using NM-algorithm, the parameters of the FOPID controller are obtained as: $K_P = 99.563, K_I = 96.239, K_D = 5.7655, \lambda = 0.61758$ and $\mu = 0.51201$. Step-response of the system with FOPID controller optimized using NM-algorithm (i.e. NM-FOPID) is compared with ZN-PID in Figure 3.5. Frequency response of the system with NM-FOPID is also shown in Figure 3.6.

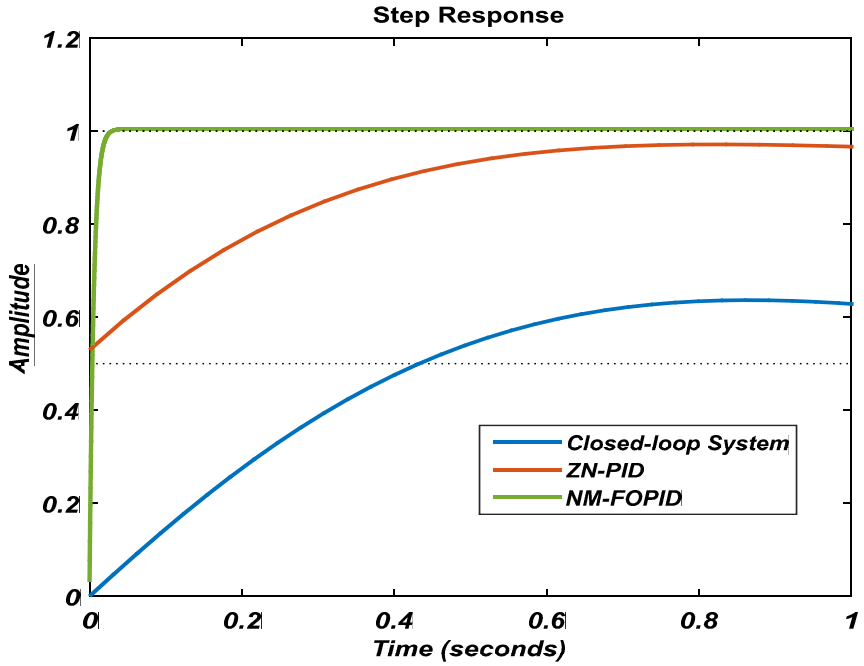

Fig. 3.5. Step-response comparison of ZN-PID and NM-FOPID

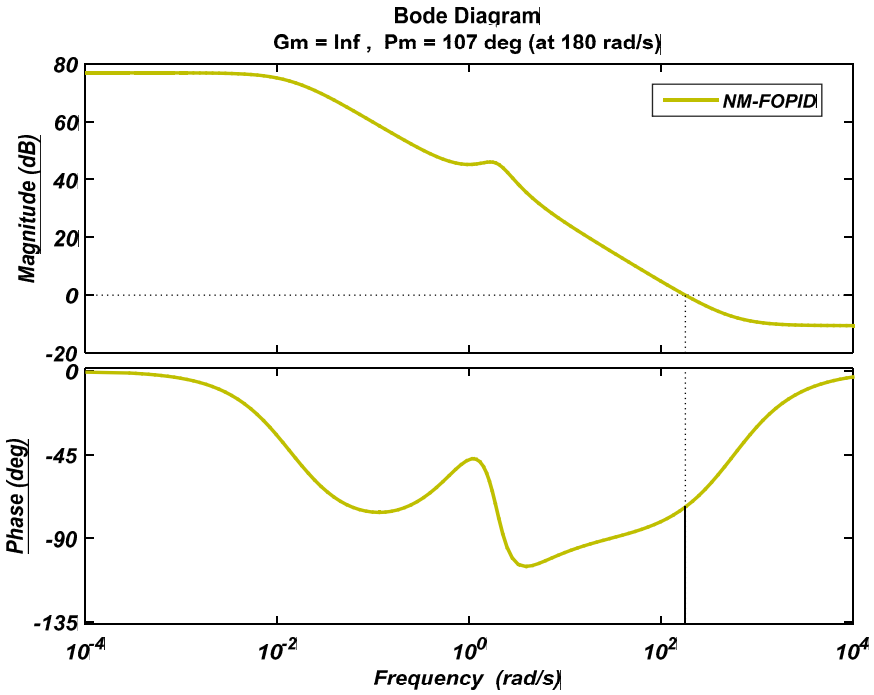

Fig. 3.6. Frequency response of the system with NM-FOPID

Table 3.1 Comparison of performance characteristics of ZN-PID and NM-FOPID

Controller	Rise-time	Settling-time	Peak Overshoot	Gain Margin	Phase Margin
ZN-PID	0.5491	3.2580	0.9997	∞	∞
NM-FOPID	0.01598	0.02642	0.7313	∞	107

Figure 3.5 support the NM-FOPID controller that fulfils all the design requirements except the phase margin of the system which is larger than the required range. The performance characteristics of both the controllers NM-FOPID and ZN-PID are compared in Table 3.1 and the performance of former is obtained to be better.

3.3.2 Design of FOPID controller for systems with time delay

In this section two varied time delay systems are considered to validate the performance of the algorithm for different types of dead time systems.

3.3.2.1 Second order system with time delay

Consider, a second order system with time delay [59]. The continuous time transfer function of the open loop system is given as:

$$G(s) = \frac{ke^{-0.2s}}{2s^2 + 3s + 1} \tag{3.7}$$

where $0.5 < k < 2$. Let $k = 0.5$.

The objective of the optimization is to design a controller to achieve the following requirements:

- $Gain\ margin\ >\ 6\ dB$
- $Phase\ margin > 51°$.
- $Flat\ phase\ at\ w = 0.5\ rad/sec.$
- $Settling\ time\ <\ 10\ sec.$

- $Peak\ overshoot\ < 24\%$

Approximation of delay term in Equation 3.7 is needed for simplicity in designing the controller. First order Pade's approximation is used and the resultant transfer function becomes:

$$G(s) = \frac{-0.5s + 5}{2s^3 + 23s^2 + 33s + 10} \tag{3.8}$$

The response of the closed-loop system shown in Figure 3.7 is over-damped and depict a steady-state error of 67%. Therefore, in order to fulfil all the design requirements an effective controller is required.

Similar to the previous case a classical PID controller is designed using ZN-method to control such a sluggish system.

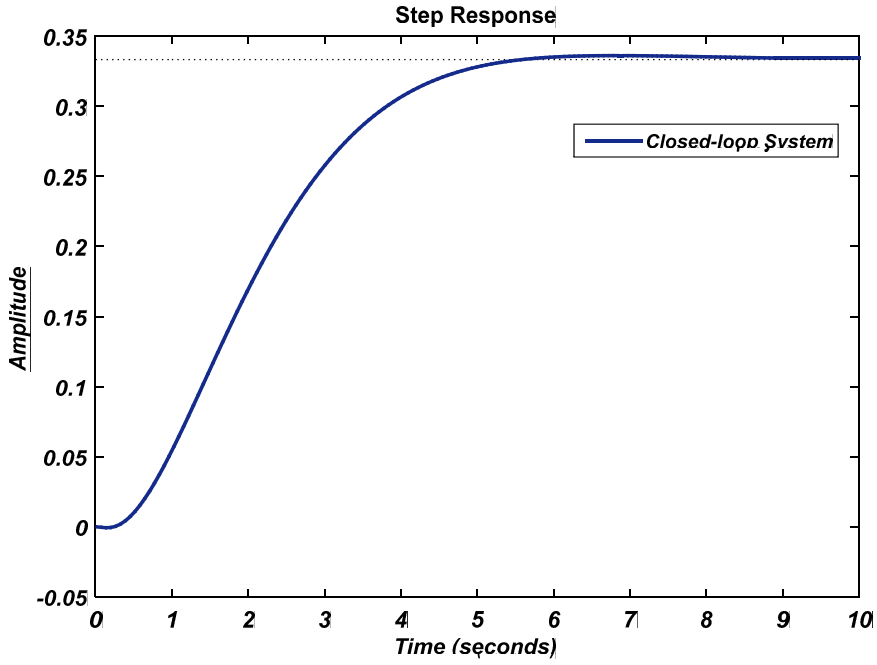

Fig. 3.7. Step response of the closed-loop time-delayed system without controller.

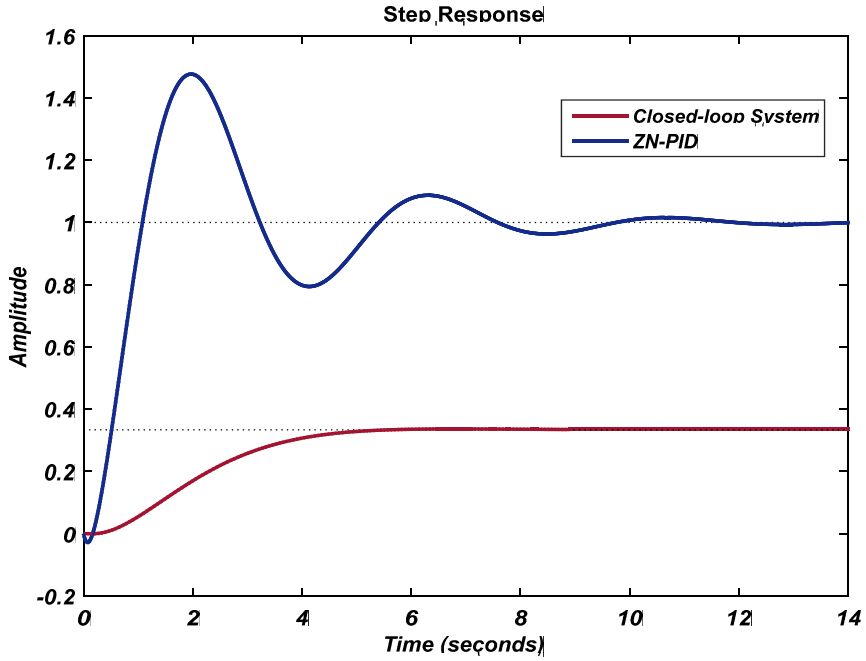

Fig. 3.8. Step response comparison of the time-delayed system ZN-PID controller and system without controller.

Figure 3.8 present the classical PID controller designed using ZN-method (i.e. ZN-PID) where the steady state error of the system reduces but the system start oscillating and the settling time increases.

Further, an FOPID controller is designed using NM-algorithm. After optimization using NM-algorithm, the parameters of the FOPID controller are obtained as: $K_P = 2.5515, K_I = 2.4342, K_D = 8.2837, \lambda = 0.51094$ and $\mu = 0.50076$. The step response of the closed loop system is compared with ZN-PID in Figure 3.9.

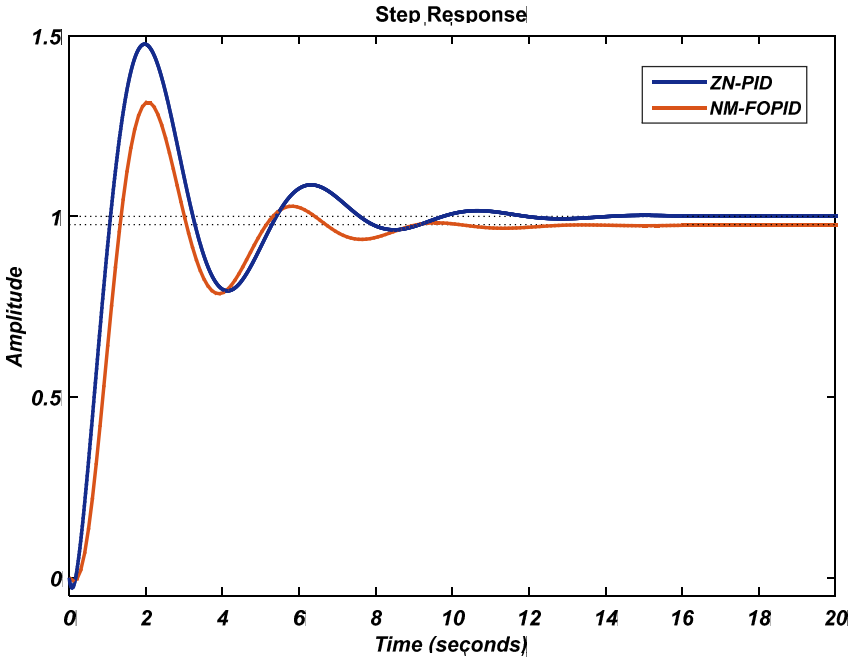

Fig. 3.9. Step response comparison of the time-delayed system with ZN-PID and NM-FOPID controller.

Table 3.2 Comparison of performance characteristics of time-delayed system with ZN-PID and NM-FOPID

Controller	Rise-time	Settling-time	Peak Overshoot
ZN-PID	0.6871	9.2096	47.6680
NM-FOPID	0.7799	8.4589	34.6049

Performance characteristics of both the controllers are compared in Table 3.2 offering an improved performance of the NM-FOPID controller.

3.3.2.2 Non-minimum phase system with time delay

The internal stability is a basic requirement for any practical closed-loop system which can be verified by testing the controllability and observability grammians of the system. In general control theory concept, the Non-Minimum Phase (NMP) is used to define a

class of systems which is governed by unstable internal dynamics. Internal dynamics are not included in control design.

Various definitions of NMP-system are also available in the literature are:

- A system is said to be NMP-system if it is causal and stable and its invers are causal and unstable [159].
- A system having zeros in the right-half s-plane (RHP) or time delays or both is said to be NMP-system.
- A system having either a zero or a pole in the right-halp s-plane is defined as NMP system.
- A zero in the right half-plane of a linearized system is a necessary and sufficient condition for the nonlinear system to be non-minimum phase [159].
- The system having both pole and zero in the right half plane is an unstable NMP-system whereas the system having only zero in the RHP is a stable NMP-system.

The practical examples of NMP system include:

- Aircraft trajectory control
- Continuous stirred tank reactor
- Water heating system and many more.

Nature of NMP systems is analogous to that of all-pass filters. As in all-pass filters every zero in the right-half side of the s-plane is the mirror image of the a stable pole in the left-half side of the plane, the generalized transfer fucntion of the NMP system can be written as:

$$G(jw) = \frac{1 - jwT}{1 + jwT} \tag{3.9}$$

Hence, the magnitute and phase of $G(jw)$ in Equation 3.9 are :

$$|G(jw)|=1 \tag{3.10}$$

$$\angle G(jw) = -2\tan^{-1}(\mathrm{wT}) \tag{3.11}$$

From Equation 3.10 and 3.11 it is clear that the magnitute of the NMP-system given here is always unity but the phase varies between 0° to -180° as w is increased from zero to infinity. The system becomes more complex when it is having a long dead-time. Transport lag normally exist in thermal, hydraulic and pneumatic systems. Additionally, the transport lag or dead-time creates an excessive phase lag with no attenuation at high frequency.

Let a single-input single-output NMP-system with time-delay be given by the transfer function as [160]:

$$G_{NMP}(\mathrm{s}) = \frac{0.1}{s(s+1)(0.5\mathrm{s}+2)(0.1\mathrm{s}+2)} e^{-8s} \tag{3.12}$$

The 1st order Pade's approximation of Equation 3.12 gives:

$$G(s) = \frac{-0.1s + 0.025}{0.05s^5 + 0.6625s^4 + 1.763s^3 + 1.4s^2 + 0.25s} \tag{3.13}$$

The step-response of the closed-loop NMP-system given by Equation 3.13 is sluggish in nature and have a large settling time of 82.5 sec. The system represent a maximum overshoot of about 37.25% as shown in figure 3.10. Hence, it desires an appropriate controller to improve the time-domain performances of the system.

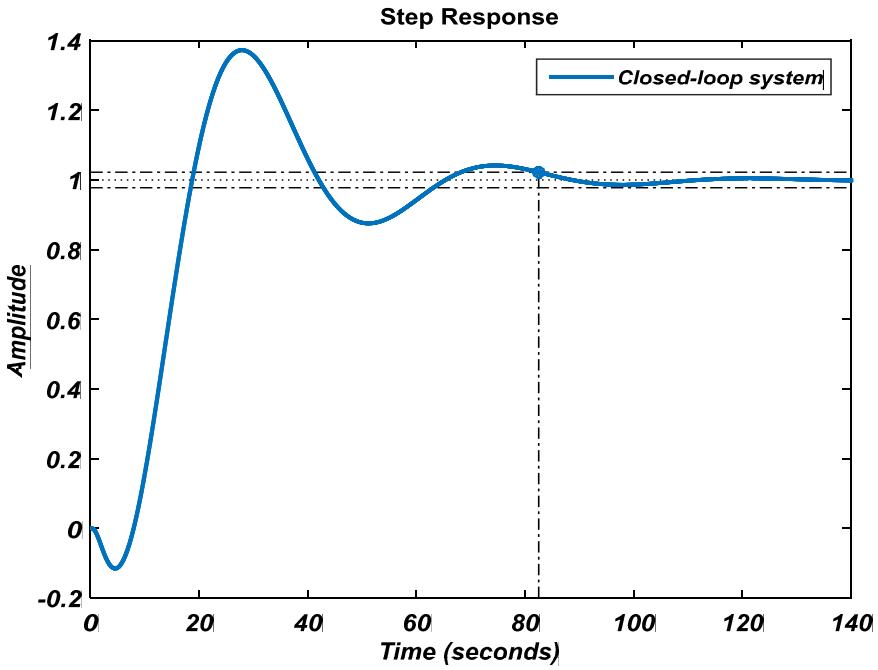

Fig. 3.10. Step response of the closed-loop NMP-system without controller.

At first, design a classical PID controller using ZN-technique (ZN-PID) using *sisotool* in MATLAB. The step response of NMP-system with ZN-PID controller is shown in Figure 3.11 which shows a faster response as compare to the system without controller. as depicted in the figure, there is no significant improvement in the performance characteristics of the system.

Further**,** an FOPID controller is designed and optimized using NM-technique (i.e. NM-FOPID) that results controller parameters as: $K_P = 1.2525, K_I = 0.0011, K_D = 6.999, \lambda = 0.109$ and $\mu = 1.103$. The step response of the NMP-system with NM-FOPID is compared with the response of the closed-loop system in Figure 3.12.

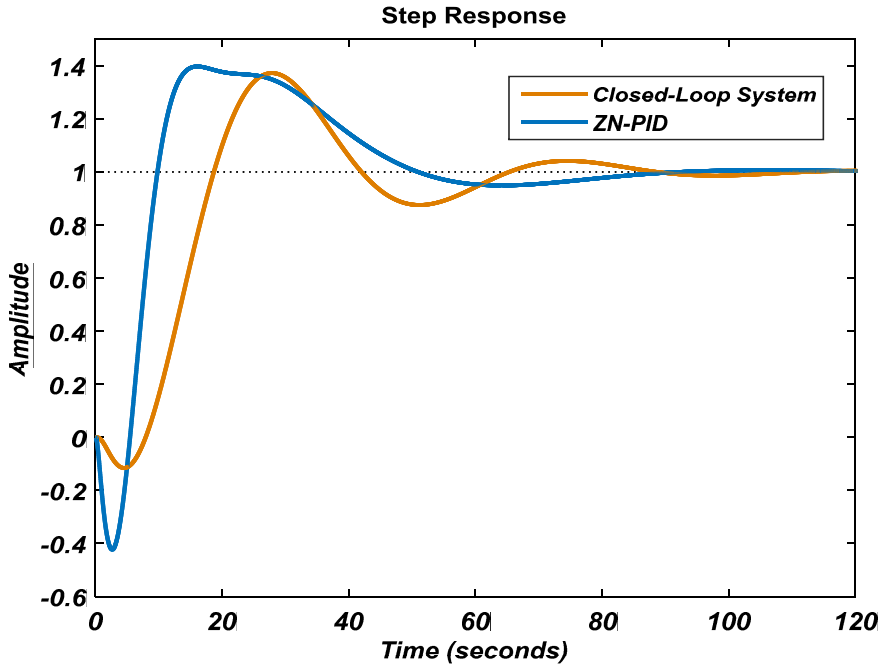

Fig. 3.11. Comparison of step response of the NMP-system with ZN-PID controller and the system without controller.

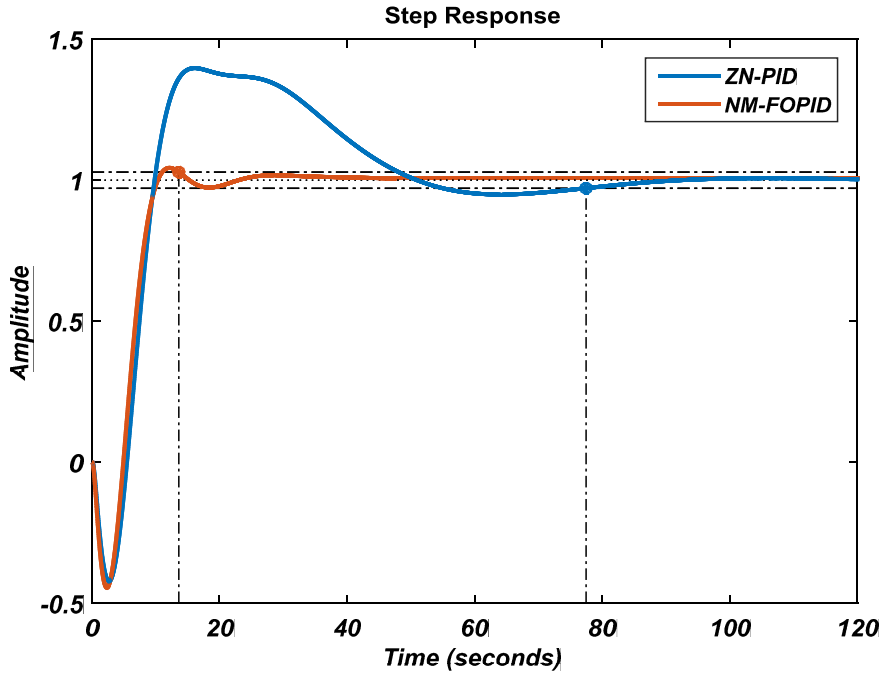

Fig. 3.12. Comparison of step response of the NMP-system with NM-FOPID and ZN-PID controller.

In Figure 3.12, it is observed that the performance of NMP-system with NM-FOPID controller offer faster and much improved performance than the classical ZN-PID controller. Comparison of performance characteristics of the NMP-system with both the controllers is tabulated in Table 3.3.

Table 3.3 Comparison of performance characteristics of NMP-system with NM-FOPID and ZN-PID.

Controller	Rise-time	Settling-time	Peak Overshot
ZN-PID	3.3664	77.4635	39.7292
NM-FOPID	3.8213	13.6168	4.3293

3.3.3 Design of an FOPID controller for magnetic levitation system

Magnetic levitation system (MLS) is an electromechanical device that hang ferromagnetic materials in air space using electromagnetism. The Magnetic levitation (Maglev) technology is attractive due to it's capability to eliminate energy losses in the form of friction due to mechanical contact. Concentrated on friction reduction, the MLS has various engineering applications such as magnetic bearings, aerospace shuttles, high-precision positioning platforms, and fast maglev trains.

The highly unstable and nonlinear MLS consist of an electromagnet coil, a metallic iron ball and an IR position sensor. The position of metallic iron ball is sensed by an IR sensor which separates the vertical movement of the ball from the horizontal one. The minimum and the maximum distance of the ball from the electromagnetic coil are reserved between 0.5 cm to 0.25 cm. The main purpose in MLS is to balance the weight (gravitational force) of the ball by the magnetic force applied by the electromagnetic coil. Thus, the current in the electromagnetic coil provide a direct control on ball. The position of the ball is indirectly controlled by applying controlled voltage across the electromagnet terminals. Thus, the voltage applied across the electromagnet

terminals provide an indirect control of the ball position [161]. The schematic block diagram of the MLS with FOPID controlled is shown in Figure 3.13 [162].

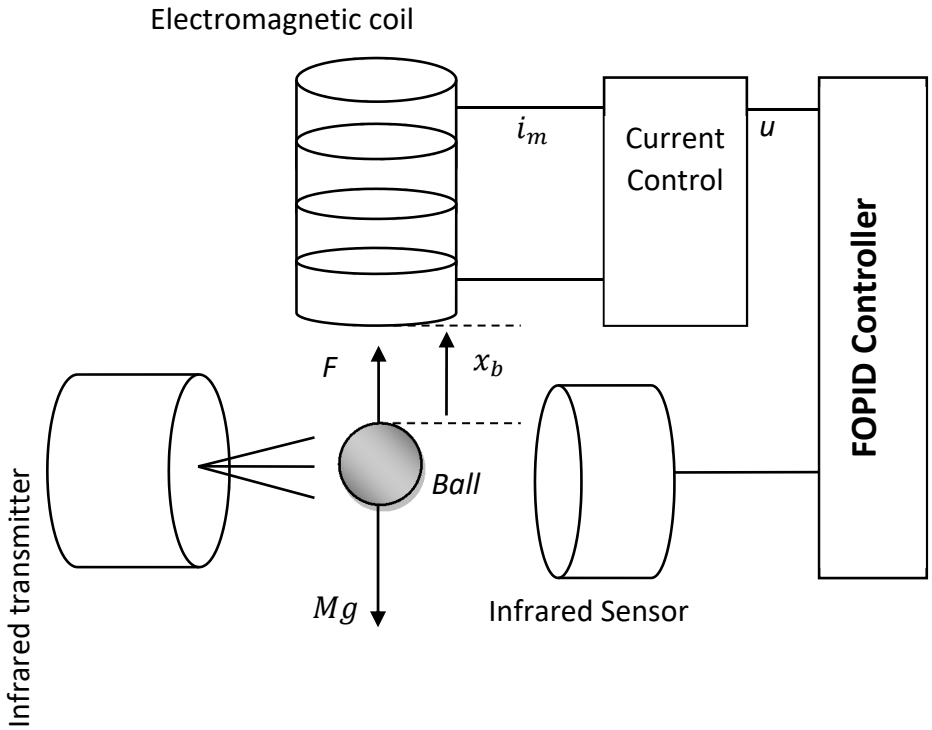

Fig. 3.13. Magnetic levitation system

The movement of the metal ball in the air space is given by [163]:

$$F = Mg - K_m \left(\frac{i_m}{x_b} \right)^2 \tag{3.14}$$

where i_m is the current in electromagnetic coil (*Ampere*), x_b is the distance of the ball from the electromagnetic coil (m), g is the gravitational constant (m/sec^2), K_m is the magnetic force constant of electromagnet and ball pair, M is the mass of the metal ball (kg).

According to the Newton's second law of motion the force F in Equation 3.14 can be written as:

$$F = \frac{d^2 x_b}{dt^2} \tag{3.15}$$

Hence from Equation 3.14, the differential equation of the MLS is given by:

$$M \frac{d^2 x_b}{dt^2} = Mg - K_m \left(\frac{i_m}{x_b} \right)^2 \tag{3.16}$$

The value of coil current and the position of the metal ball at the operating point is derived by allowing $\frac{d^2 x_b}{dt^2} = 0$ in Equation 3.16 gives:

$$x_{b_{ss}} = \sqrt{\frac{K_m}{Mg}}\, i_{m_{ss}} \tag{3.17}$$

where $x_{b_{ss}}$ and $i_{m_{ss}}$ are the value of position of metal and current of electromagnetic coil at the operating point.

This coil current is sufficient in theoretical sense to levitate the position of the metal ball to the desired location but it fails practically due to variation at operating point because of external disturbances, parameter uncertainties and others. Therefore, there is a requirement of an efficient controller which is capable of handling such irregularities of the system. The MLS is linearized by taking the approximation of x_b and i_m as:

$$x_b(t) \triangleq \hat{x}_b + x_{b_{ss}} \tag{3.18}$$

$$i_m(t) \triangleq \hat{\imath}_m + i_{m_{ss}} \tag{3.19}$$

where $\hat{x}_b$ and $\hat{\imath}_m$ are the variations of metal ball position and coil current around the operating point. Thus the dynamic equation of the MLS is written as:

$$M \frac{d^2 \hat{x}_b}{dt^2} = Mg - K_m \left(\frac{\hat{i}_m + i_{m_{ss}}}{\hat{x}_b + x_{b_{ss}}} \right)^2 \tag{3.20}$$

Now, linearizing the above system using Taylor's series expansion and assuming that $\hat{x}_b \gg x_{b_{ss}}$, and $\hat{\imath}_m \gg i_{m_{ss}}$

$$\frac{d^2\hat{x}_b}{dt^2} = \frac{1}{M}\left\{\frac{\partial}{\partial \hat{x}_b}\left(Mg - K_m\left(\frac{\hat{i}_m + i_{m_{ss}}}{\hat{x}_b + x_{b_{ss}}}\right)^2\right)\Bigg|_{\hat{x}_b=0,\hat{i}_m=0} \hat{x}_b + \frac{\partial}{\partial \hat{i}_m}\left(Mg - K_m\left(\frac{\hat{i}_m + i_{m_{ss}}}{\hat{x}_b + x_{b_{ss}}}\right)^2\right)\Bigg|_{\hat{x}_b=0,\hat{i}_m=0} \hat{i}_m\right\} \tag{3.21}$$

Therefore,

$$\frac{d^2\hat{x}_b}{dt^2} = \frac{1}{M}\left(\frac{2K_m i_{m_{ss}}^2}{x_{b_{ss}}^3}\hat{x}_b - \frac{2K_m i_{m_{ss}}}{x_{b_{ss}}^2}\hat{i}_m\right) \tag{3.22}$$

By taking Laplace transform the transfer function of the MLS is obtained as:

$$G(s) = \frac{\hat{X}_b(s)}{\hat{I}_b(s)} = -\frac{K_2}{s^2 - K_1} \tag{3.23}$$

where $K_1 = \frac{2K_m i_{m_{ss}}^2}{M x_{b_{ss}}^3}$ and $\frac{2K_m i_{m_{ss}}}{M x_{b_{ss}}^2}$ with $M = 0.002\ kg,\ g = 9.81\ m/sec^2$. At the equilibrium point of MLS the feedback makes $\left[x_{b_{ss}} = -1.5\ V, i_{m_{ss}} = 0.8\ A\right]$. Therefore, the open loop transfer function of the MLS is:

$$G(s) = \frac{-24.5250}{s^2 + 13.08} \tag{3.23}$$

The open-loop poles of the system are located on the imaginary axis at $s = \pm j3.6166$. Thus, the system lead to instability or have sustained oscillations. The closed-loop poles are located at $s = \pm 3.3823$. The open-loop step response of the MLS is shown in Figure 3.14.

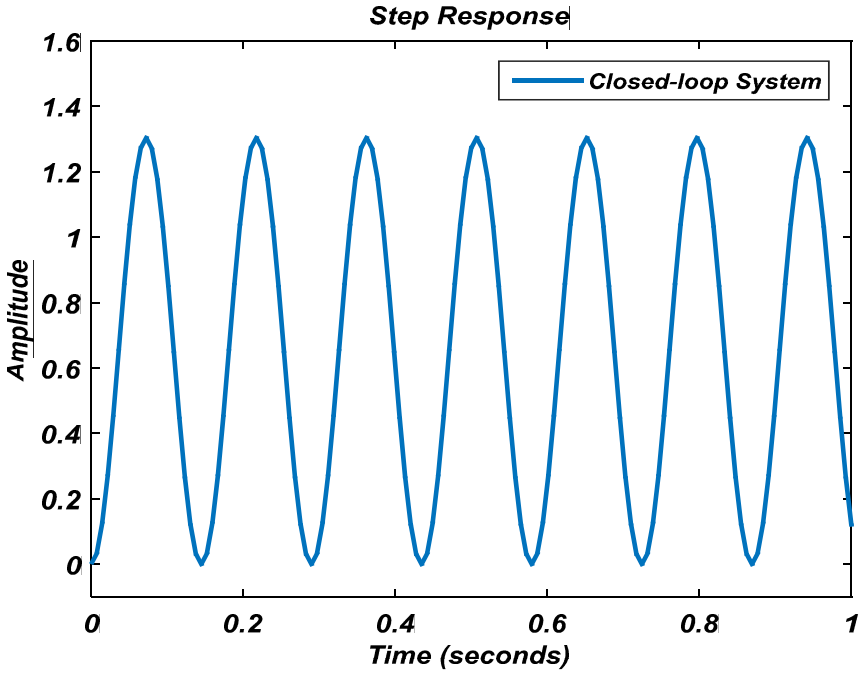

Fig. 3.14. Step response of the open-loop MLS without controller

The major difficulty is the instability of the closed-loop system with one closed-loop pole lying in the right-half of the s-plane. Therefore, an efficient controller is needed that can stabilize the position of the metal ball to levitate in the air space.

Here, firstly a classical PID controller is designed using ZN-technique and trial and error method (TE-PID) in MATLAB. The step response of MLS with ZN-PID and TE-PID controller is shown in Figure 3.15. Among both the controllers TE-PID present a faster response as compared to the ZN-PID but still it lags in terms of maximum overshoot and settling time of the system.

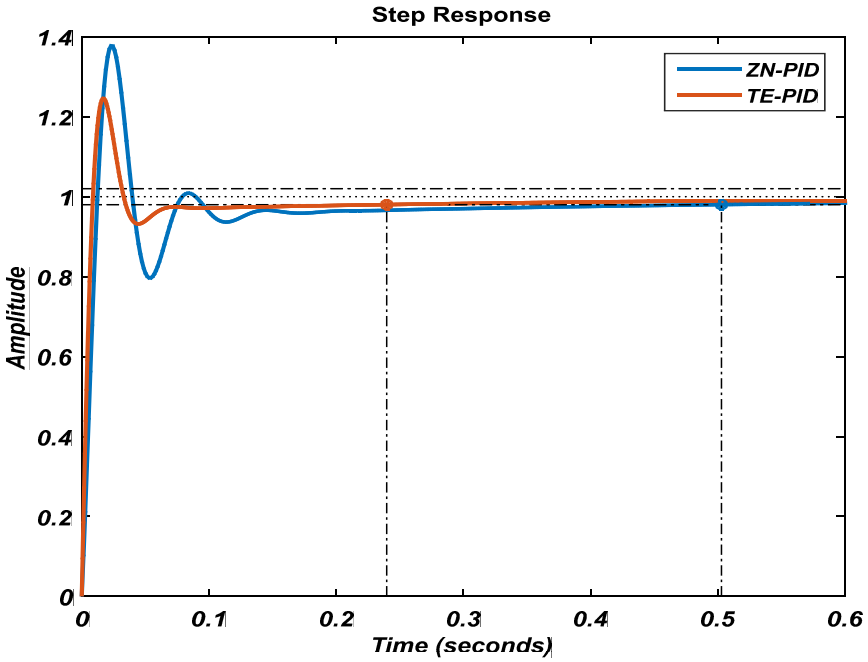

Fig. 3.15. Step response of the MLS with ZN-PID and TE-PID controllers

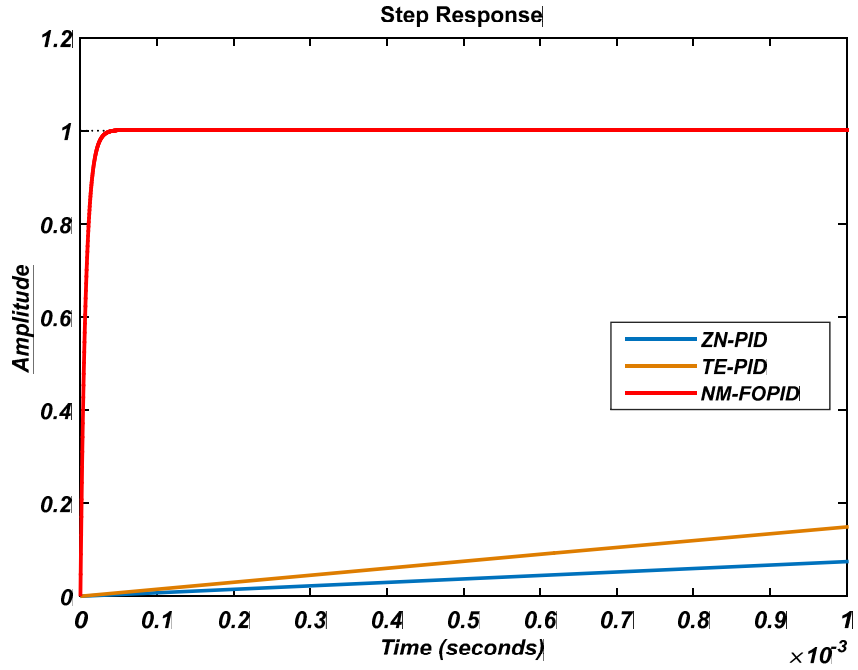

Fig. 3.16. Comparison of step response of the closed-loop MLS with NM-FOPID, ZN-PID and TE-PID controllers

Later, an FOPID controller is designed and optimized using NM-technique (i.e. NM-FOPID). The optimized value of the FOPID parameters are obtained as: $K_P = 99.057, K_I = 79.773, K_D = 180.881, \lambda = 0.9345$ and $\mu = 0.94258$. The step response of the MLS with NM-FOPID is compared with that of ZN-PID and TE-PID in Figure 3.16. The figure showcase the fulfilment of the desired performance and perform the faster control action among all three controllers.

Table 3.4 Comparison of performance characteristics of MLS with NM-FOPID, ZN-PID and TE-PID controllers.

Controller	Rise-time	Settling-time	Peak Overshoot
ZN-PID	0.0096	0.503	37.6922
TE-PID	0.0068	0.2637	22.1133
NM-FOPID	$1.46 * 10^{-5}$	$2.58 * 10^{-5}$	0.0976

The performance characteristics of all the controllers are compared in Table 3.4 offering better performance by NM-FOPID controller as compared to the other two.

3.3.4 Design of an FOPI controller for a Non-monotonic phase system

Feedback control system maintains a prescribed relationship between the reference input and the desired output. The difference between the reference input and final output of the system is known as error of the system and minimized using controller. In frequency response the compensation of a linear continuous (or discrete) time invariant (LTI) system is done by applying a negative feedback control. In classical control design the phase margin of a system having monotonically decreasing phase inside the bandwidth is calculated as the distance between the open-loop phase at the gain crossover frequency and the stability limit of −180°. However, the system having a left half-plane zero located near the dominant-poles (i.e minimum-phase system) shows non-monotonic phase

behavior inside the bandwidth [69]. For a closed loop system to be stable both the gain margin and phase margin must be positive. Phase margin of a closed-loop system estimate the robustness and informs how much the open-loop system phase may vary while the closed-loop system remains stable [164]. However, this theory is not valid in common practice, because even for a minimum phase system having a left half-plane zero located near the dominant- poles, its frequency response will present a non-monotonic phase.

The DC-buck regulator system, which is widely used in power electronic applications, pose the non-monotonic phase behavior inside the bandwidth. Hence, it deserve an effective controller to get the wider bandwidth, faster time response and more sensitive to noise and parameter variations.

The DC-buck regulator system is a combination of the power stage (i.e a LC low-pass filter) and a pulse-width modulation (PWM)-based controller [69]. The circuit diagram of DC-buck converter with voltage controller is given in Figure 3.17.

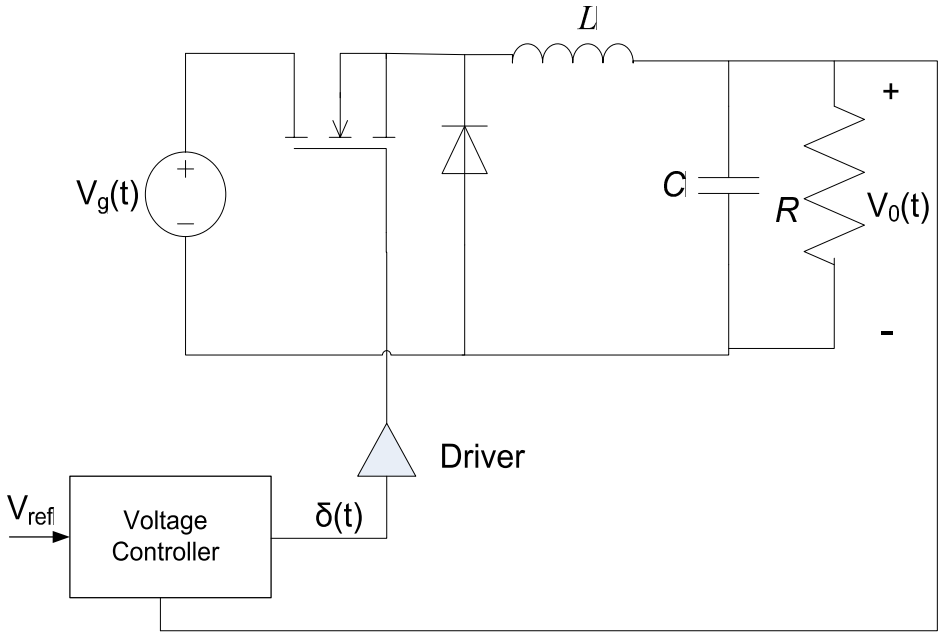

Fig. 3.17. Circuit diagram of DC-Buck Converter with a voltage controller.

The transfer function of DC-buck regulator system is written as ratio of the output (regulated voltage) to the input (PWM modulator input voltage) as:

$$G = \frac{V_{in}(1 + sR_C C)}{V_{OSC} LCs^2 + s\left(R_C C + \frac{L}{R}\right) + 1} \tag{3.25}$$

where C is output capacitance, L is output Inductance, R is load resistance, R_C is the output capacitor intrinsic resistance, V_{in} the power stage input voltage and V_{OSC} is the PWM oscillator reference voltage.

For a typical application of DC-buck regulator considered in International Rectifier, (2002) with $\mathrm{R_C} = 40\ \mathrm{m\Omega}$, the transfer function is given as:

$$G = \frac{4(1 + 1.2 \times 10^{-5})}{3 \times 10^{-9} s^2 + 3.6 \times 10^{-5} s + 1} \tag{3.26}$$

The frequency plot of the DC-buck regulator depict the non-monotonic phase behaviour near its undammed frequency. The closed-loop step response of the DC-buck regulator without any controller is also shown in Figure 3.18, which present the system to be under-damped. The response also shows a steady state error of about 20% of the desired value. Hence it requires an effective control algorithm to improve the performance of the system.

To improve the performance of the DC-buck regulator firstly a classical PI controller is designed using ZN-technique (i.e. ZN-PI), Figure 3.19 present the step response. The obtained ZN-PI controller improves the settling time and steady state error of the system but still the system is under dammed in nature and show a maximum overshoot of about 51.5%.

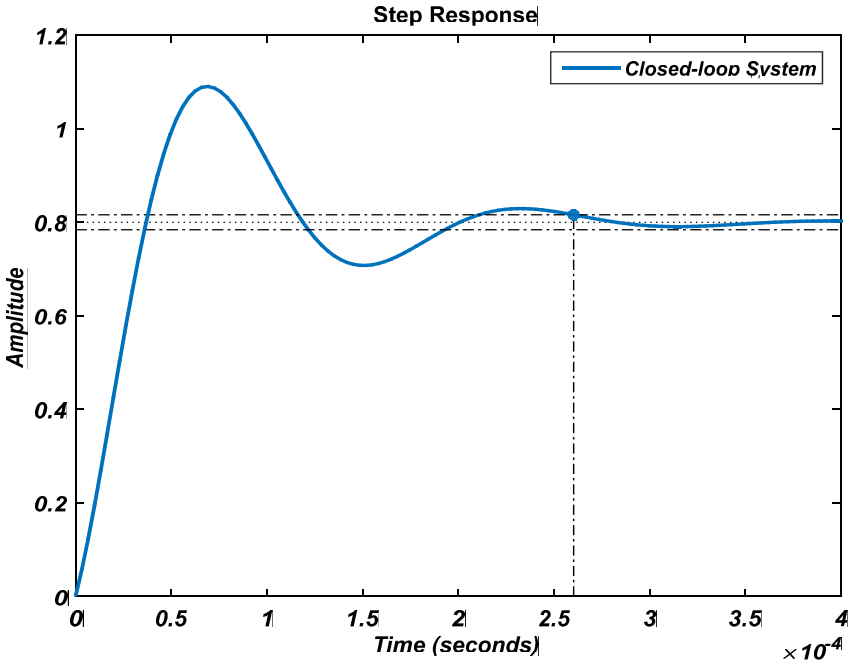

Fig. 3.18. Step response of the closed-loop DC-buck regulator without controller

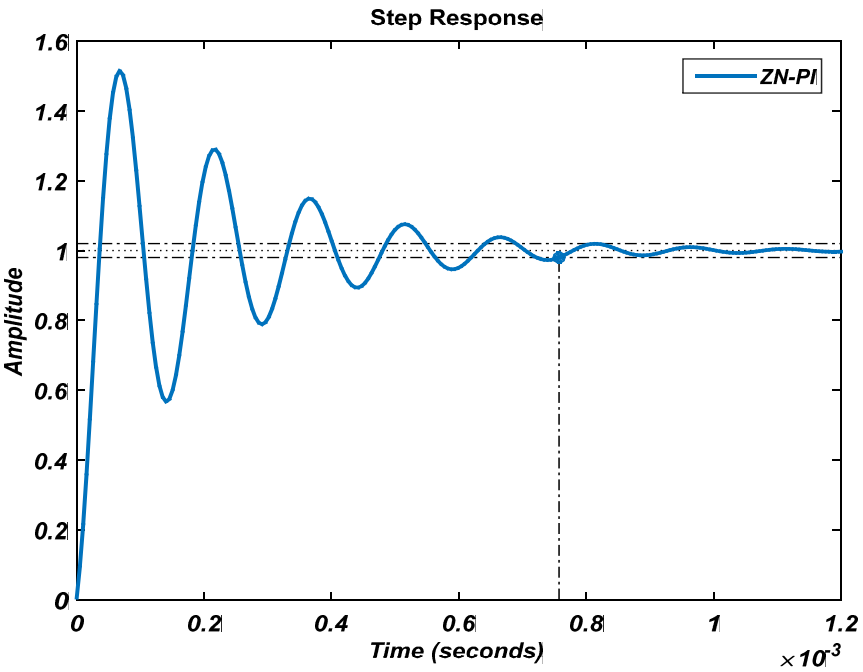

Fig. 3.19. Step response of the DC-buck regulator with ZN-PI controller

Further, an FOPI controller is design by optimizing the parameters of ZN-PI controller using NM-algorithm. The parameters of FOPI controller after optimization are obtained as: $K_P = 175, K_I = 97, \lambda = 0.81$. Step response of the DC-buck regulator system with FOPI controller optimized using NM-algorithm (i.e. NM-FOPI) is compared with the ZN-PI in Figure 3.20.

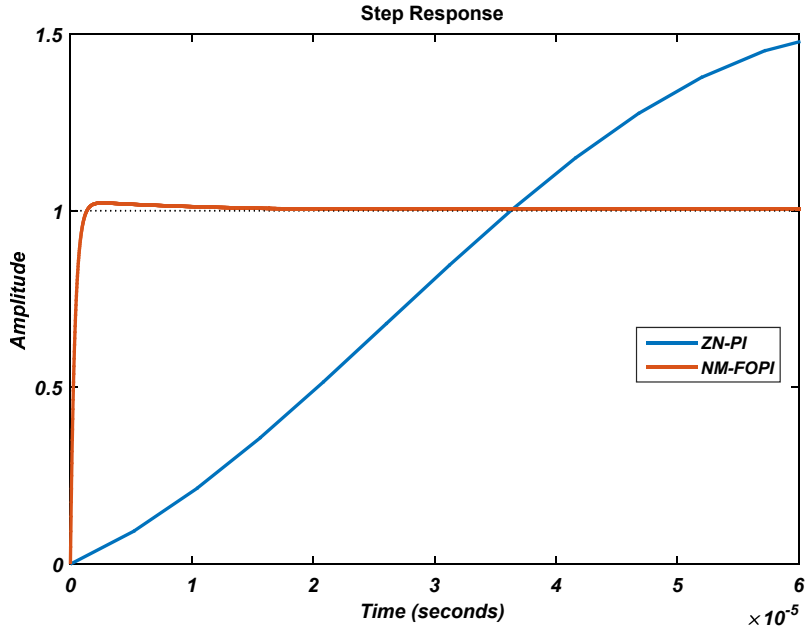

Fig. 3.20. Comparison of step response of the DC-buck regulator with ZN-PI and NM-FOPI controller

Table 3.5 Comparison of performance characteristics of DC-buck regulator with NM-FOPI, ZN-PI controllers.

Controller	Rise-time	Settling-time	Peak Overshoot	Gain Margin	Phase Margin
ZN-PI	$2.7501 * 10^{-5}$	$7.5751 * 10^{-4}$	51.5141	∞	46.9
NM-FOPI	$7.2845 * 10^{-7}$	$4.5026 * 10^{-6}$	2.2698	∞	88.5

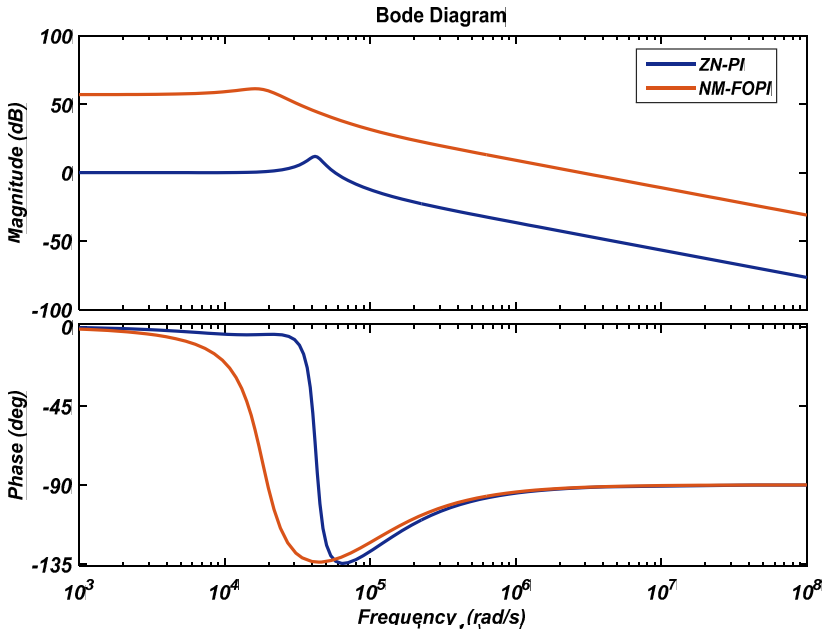

Fig. 3.21. Comparison of frequency response of the DC-buck regulator with ZN-PI and NM-FOPI controller

The Figure 3.20 support the performance of DC-buck regulator with NM-FOPI controller to be faster than the ZN-PI. The obtained controller also improves the frequency response of the system in terms of phase margin as shown in Figure 3.21. The performance characteristics of both the controllers are compared in Table 3.5 which proves the effectiveness of NM-FOPI controller over the classical one.

3.3.5 Design of FOPID controller for a spherical tank system

Various procedures in process industries commonly the liquid undergoes either a chemical treatment or mixing treatment in various tanks. In these procedures a high liquid level may trouble the equilibrium of the reaction which causes the harm to the equipment or the leakage of expensive or hazardous material. A low liquid level may create contrary consequences which disturbs the successive operations. Therefore, controlling the liquid level in tanks is very significant and common job in process industries.

Spherical tanks are extensively used in various process industries as storage tanks of fuels, cryogenic liquids, significant chemicals and other liquids. Due to gradual change in cross sectional area spherical tanks require minimum space, hence they are also used as surge tanks in between consecutive stages of processes. Because of the nonlinearity produced due to the change in cross section area, controlling of liquid level in spherical tank is very tricky. Hence, only a robust controller effectively control the level of the liquid inside the spherical tank. The experimental model of a Spherical Tank System (STS) is shown in Figure 3.22 [165].

Fig. 3.22. Experimental model of STS.

A fractional order model of STS is considered to design an optimized FOPID controller in this work. The fractional order model of a plant or system can be illustrated by a generalized n-terms linear and homogeneous fractional differential equation in time domain given in [48]. The transfer function of the STS in fractional domain is considered as [165], [166]:

$$G_F(s) = \frac{e^{-8s}}{3.5s^{0.5} + 11.5s^{0.4} + 1} \tag{3.27}$$

This fractional order system is approximated to an integer order system by Oustaloup's algorithm [47]. The approximated integer order transfer function of the system is of 26th orders. Hence, to reduce the design complexity the system is further reduced into a second order transfer function using Balanced Truncation Technique [167], [168]. The 2nd order reduced transfer function of the STS system is obtained as:

$$G = \frac{0.02537s + 7.7 \times 10^{-5}}{s^2 + 0.09176s + 9.356 \times 10^{-5}} \tag{3.28}$$

The closed-loop response of the system shown in Figure 3.23 is very sluggish and shows a large (about 0.55) steady state error. Therefore, a fast and efficient controller is needed to control the liquid level in the STS.

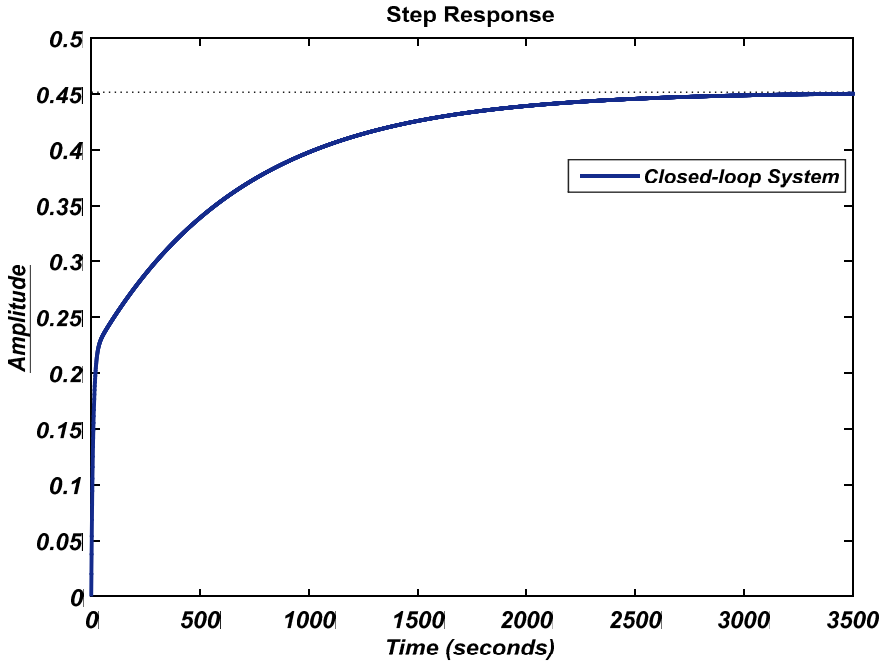

Fig. 3.23. Step response of closed-loop STS without controller.

The ZN-PID designed for the system improves the steady state performance but it fails to improve the settling time of the system as shown in Figure 3.24.

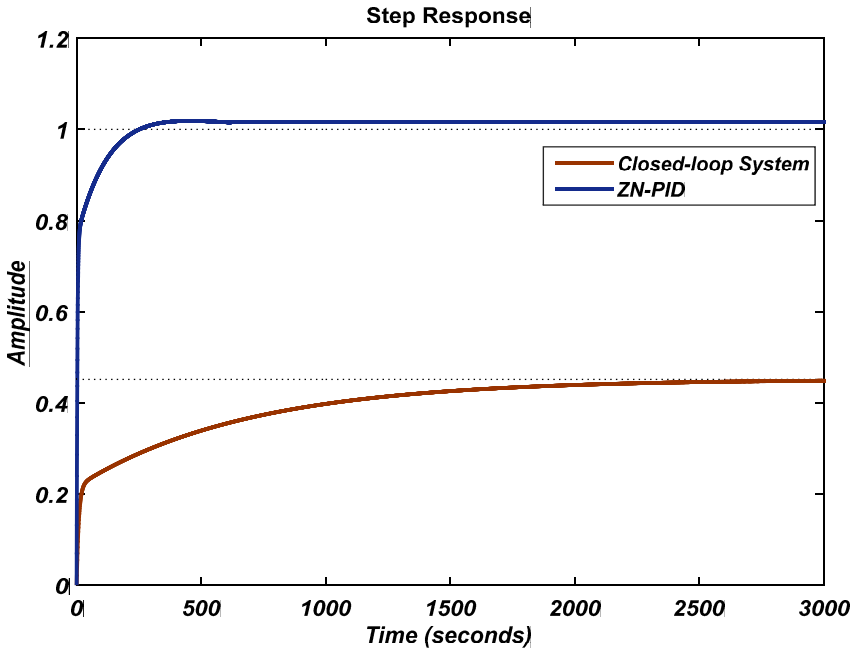

Fig. 3.24. Comparison of step response of STS with ZN-PID and system without controller.

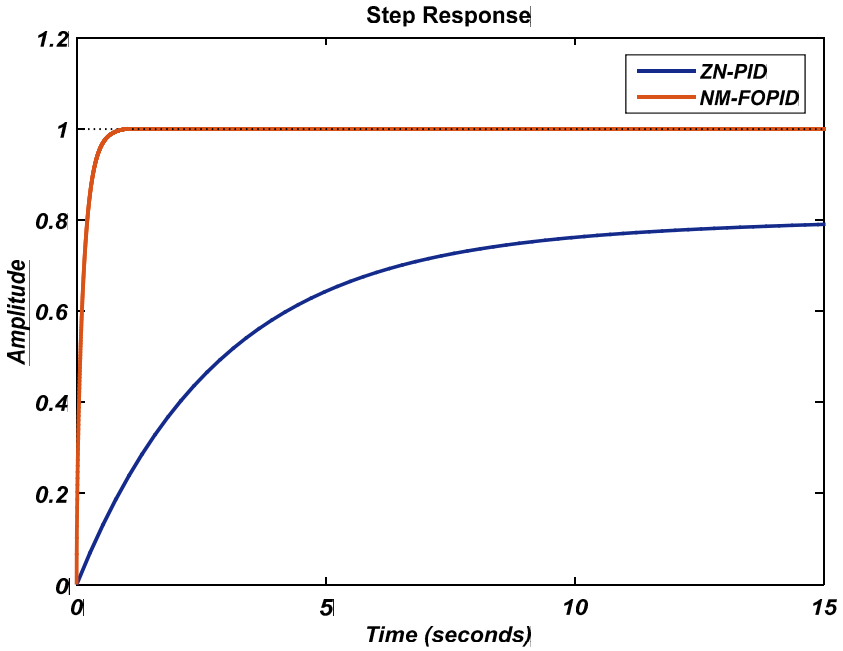

Fig. 3.25. Comparison of step response of STS with ZN-PID and NM-FOPID controllers

After optimization using NM-algorithm the parameters of FOPID controller are obtained as: $K_P = 99.38, K_I = 195.10, K_D = 49.7026, \lambda = 0.20225$ and $\mu = 0.51908$. The NM-FOPID controller improves the steady state performance and settling time of the closed-loop system as shown in Figure 3.25.

Table 3.6 Comparison of performance characteristics of STS with NM-FOPID and ZN-PID controllers.

Controller	Rise-time	Settling-time	Peak Overshoot
without controller	$1.1169 * 10^3$	$2.2103 * 10^3$	0
ZN-PID	84.644	193.0292	1.8564
NM-FOPID	0.3218	0.5910	0.1027

Performance characteristics of the STS with both controllers are compared in Table 3.6 which validates the effectiveness of the NM-FOPID controller and the proposed algorithm.

3.3.6 Design of an FOPID controller for AVR system

Power system network is mainly designed to work at a convinced frequency and terminal voltages. Any disturbances raised by a swing in the output of the turbine, deviation in load or, deviation in transmission line parameters, may cause dynamic instability within the system. These instabilities lead to overall system collapse or, it may damage any coupled equipment. The two independent control loops are designed to focus on these parameters namely the load frequency control and automatic voltage regulator (AVR). Application of AVR in power system enhances the stability of the power system and keeps the magnitude of the terminal voltage at a specified level, which is previously done by placing a capacitor in series with the power transmission lines. As per literature survey

the AVR system is found cheaper and very effective for controlling the terminal voltage of the generator [71], [147].

The AVR system is a combination of four sub-systems namely amplifier, exciter, generator, and sensor. Here for convenience, a linearized model of AVR system is considered. The schematic block diagram of the AVR system is shown in Figure 3.26. The transfer function of its each component (sub-systems) is placed in the corresponding block.

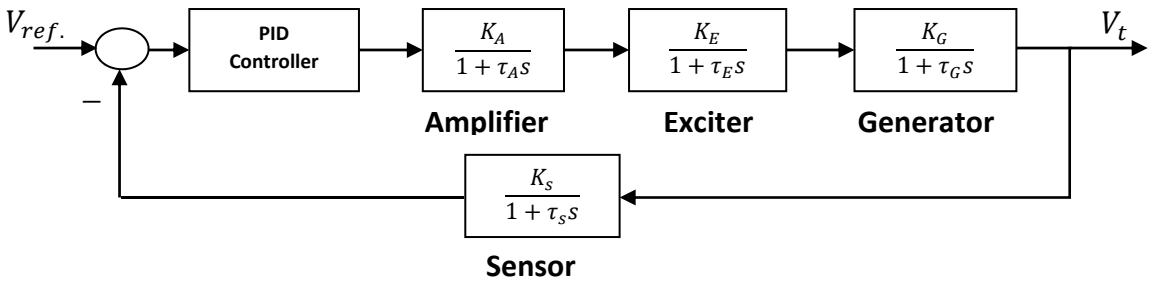

Fig. 3.26. Block diagram of an AVR system

The typical range of values of the parameters of the AVR system are as: $K_A = [10, 400]$, $\tau_A = [0.02, 0.1]$, $K_E = [1,400]$,$\tau_E = [0.4, 1.0]$, $K_G = [0.7, 1.0]$, $\tau_G = [1.0, 2.0]$, $K_s = [1.0, 2.0]$, $\tau_s = [0.001, 0.06]$. The considered parameter values are as: $K_A = 10$, $\tau_A = 0.1$, $K_E = 1$, $\tau_E = 0.4$, $K_G = 1$, $\tau_G = 1$, $K_s = 1$, $\tau_s = 0.01$. Hence the closed-loop transfer function of the AVR system without controller is written as:

$$G_{AVR} = \frac{V_t(s)}{V_{ref.}(s)} = \frac{0.1s + 10}{0.0004s^4 + 0.045s^3 + 0.555s^2 + 1.51s + 11} \tag{3.29}$$

From Equation 3.28, the calculated two real poles are located at $s_1 = -99.9712$ & $s_2 = -12.4892$ and two complex poles are at $s_{3,4} = -0.5198 \pm 4.6642i$ and one zero at $z = -100$. The step response of the AVR system shown in Figure 3.27, shows the oscillating behavior which proves the under-damped nature of the system.

Moreover, the phase plot in Figure 3.28 shows very small gain margin (GM) and phase margin (PM). Therefore, an efficient controller is desired to improve the overall performance of the system.

The ZN-PID controller designed using MATLAB improves the steady state error of the AVR system but fail to improve the under damped behavior of the system as shown in Figure 3.29.

The NM-algorithm give optimized value of the parameters of FOPID controller as: $K_P = 27.564, K_I = 0.4492, K_D = 1.3934, \lambda = 0.8085$ and $\mu = 1.7465$. The NM-FOPID controller improves the steady state performance of the system as well as settling time of the closed-loop system as shown in Figure 3.30.

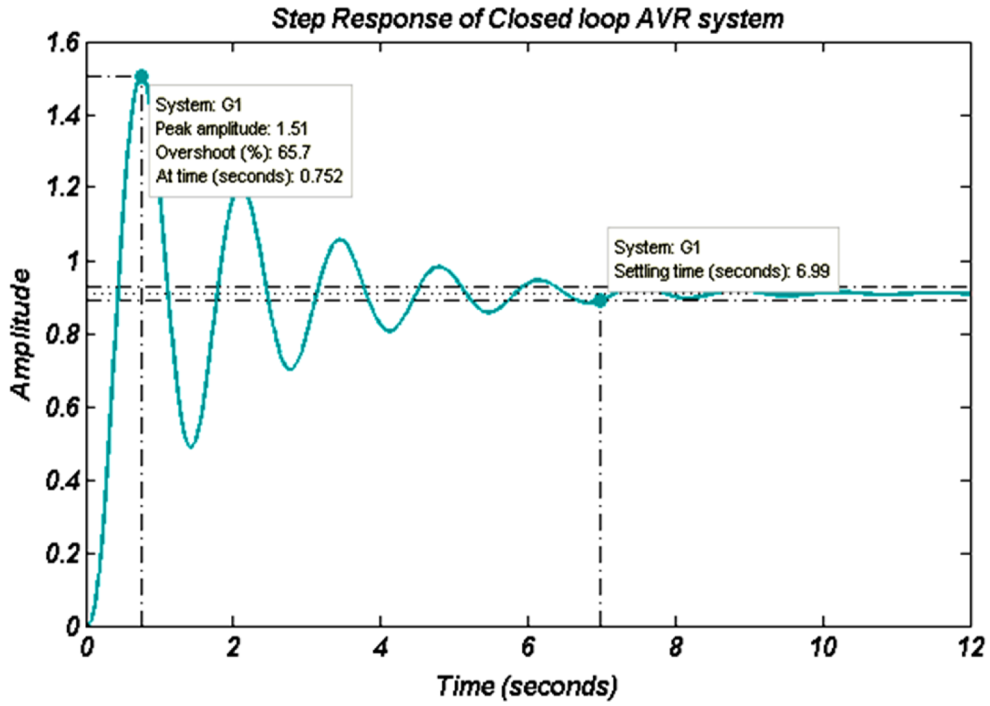

Fig. 3.27. Step response of the closed-loop AVR system without controller

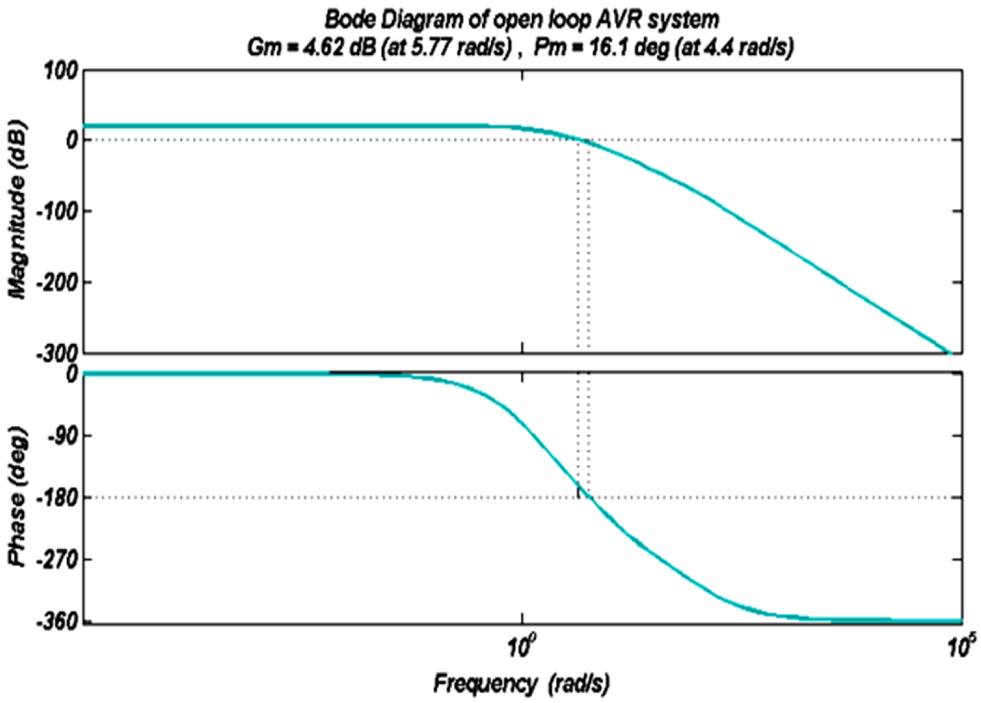

Fig. 3.28. Frequency response of open-loop AVR system without controller

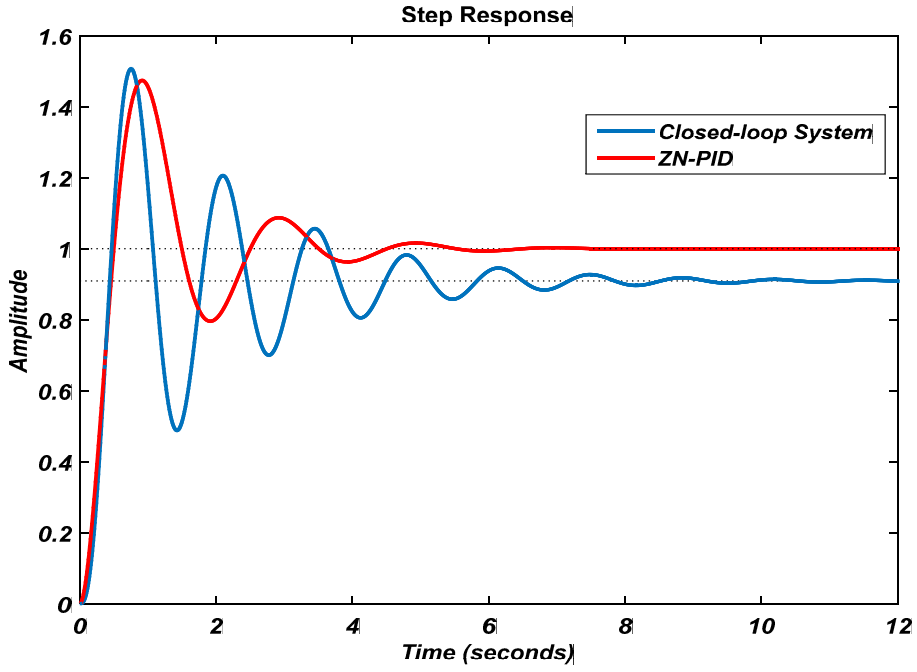

Fig. 3.29. Comparison of step response of AVR system with ZN-PID and system without controller.

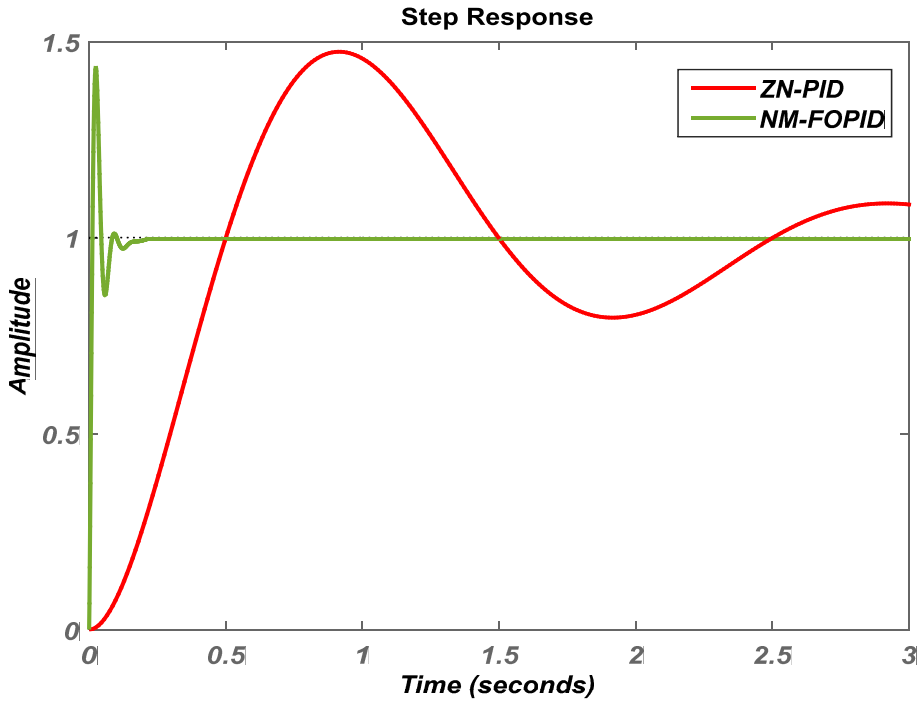

Fig. 3.30. Comparison of step response of AVR system with ZN-PID and NM-FOPID controller.

Table 3.7 Comparison of performance characteristics of AVR system with NM-FOPID and ZN-PID controllers.

Controller	Rise-time	Settling-time	Peak Overshoot
ZN-PID	0.3435	4.2656	47.3931
NM-FOPID	0.0090	0.1393	43.2353

The performance characteristics of the AVR system with NM-FOPID controller shown in Table 3.7 proves the faster performance of the proposed controller and effectiveness of the algorithm as well.

3.4 Summary

This chapter illustrated the design of FOPID controller and optimization of their parameters using NM-algorithm. Effectiveness of the algorithm is validated by designing the FOPID controller for different types of system and comparing the results with

classical PID controller designed using ZN-technique. A new evolutionary algorithm is discussed in the next chapter for optimization of FOPID controller parameters.